Design and Analysis of a Self-Holding Three-Position Electric Tubular Actuator

Petrov Ilya, Immonen Paula, Pyrhönen Juha

DOI: 10.1109/TIE.2020.3013773

Design and Analysis of a Self-Holding Three-Position Electric Tubular Actuator

Ilya Petrov, Paula Immonen, and Juha Pyrhönen, *Senior Member, IEEE*

***Abstract*—A self-holding three-position electric tubular actuator (SHTPETA) is described in the paper. The proposed linear actuator can be applied in a clutch system, where it is necessary to change certain mover positions over time. Other potential applications of such actuators can be shift of gears, coupling (decoupling) of various moving (rotating) mechanisms, or electromagnetic valves. The self-holding force of the proposed SHTPETA is achieved by the reluctance force between the armature and mover cores, where a magnetic flux is excited by a permanent magnet located in the armature and an excitation current is not needed, whereas the moving force is determined by the DC voltage (current) applied to two coils located in the stationary part of the SHTPETA. The paper proposes a relatively fast and simple approach for the SHTPETA design process based on the required forces and moved distance.**

***Index Terms*—Permanent magnet machines, Electric machines, Actuators.**

I. Introduction

ELECTRIFICATION of passenger cars by applying a hybrid electric topology or a fully electric system often involves development of an electric propulsion motor that is capable of operating over the whole speed range by using only one fixed gear ratio [1]. However, it is commonly understood that also with a pure electric propulsion system it is advisable to use a transmission system with a variable gear ratio, which helps to improve the overall operating efficiency of the electric propulsion system over the whole thrust/speed range and enhance the dynamic characteristics of the vehicle [2], [3]. This is especially pronounced for torque-demanding vehicles, such as sport racing cars [4] and off-road machines [5]. Apart from hydraulic or electrohydraulic systems (typically used in transmission systems because of their high force density), switching of the gear ratio can also be implemented by purely electric actuators [6]. Such systems are often referred to as shift-by-wire systems allowing to improve the human interface with the power elements of the vehicle, thereby making it more convenient for daily use and more flexible at the development stage [7]. Further, an electric actuator helps to reduce the energy loss caused by oil pumps that run continuously by the internal combustion engine (ICE) when a hydraulic system is used. In [8], a linear electromagnetic actuator was proposed for direct shifting of gears in a vehicle transmission. The developed actuator satisfied the requirements in terms of maximum stroke length, dynamic response, and force provided over the whole stroke length. However, the location of the magnets on the mover could reduce the reliability of the system because of the presence of magnetic swarf in the surrounding environment, which would require sealing of the mover. Moreover, the proposed control had to be implemented with power electronics (pulse width modulation) along with certain PD controller parameters and desirably with knowledge of the mover position to capture its middle (neutral) position. Therefore, a new more reliable electromagnetic actuator with a simpler control had to be developed for a similar application (switching the gear ratio in the transmission system) having self-holding positions; however, compared with the voice-coil-like structure described in [9], the self-holding force must be stronger (above 50 N), and not two but three self-holding positions should be achieved. A large proportion of short-distance linear actuators operate on the voice-coil principle [10]–[14]. They provide almost linear force over the whole stroke displacement. However, these linear actuators need a winding in the mover, which complicates the voltage supply system and degrades its reliability. Further, this topology does not require the mover to be retained in certain positions by means of no-load electromagnetic forces, and if no-load positioning is needed, it is implemented by applying retaining spring(s). A similar principle is applied in linear tubular short-stroke motors that are used for reciprocating loads, such as vapor compressors [15], [16]. However, these actuators do not have electromagnetic self-holding positions either, which are needed to keep the mover at a predefined distance.

A three-position actuator with self-holding forces was proposed in [17]. However, as a result of placing the magnets into the mover and a special magnet magnetization direction, which directly opposes the field induced by the armature, this construction could lead to the risk of irreversible demagnetization at temperatures above 70° C, because the field strength over the magnet could reach 1 MA/m in such a structure [18]. Further, when the magnets are positioned in the mover, it is more challenging to remove the heat from them. Thus, a parallel magnetization direction of the magnet and the armature reaction should be preferred to decrease the eddy current losses in the magnets and to reduce the opposing fields from the armature to the magnet to allow the structure to work at higher temperatures without a risk of irreversible

Manuscript received May 07, 2020; revised June 09, 2020; accepted July 16, 2020. This work was supported in part by the Academy of Finland under grant 311248.

Ilya Petrov, Paula Immonen and Juha Pyrhönen are with the Laboratory of Electric Drives Technology, LUT University, Lappeenranta, 53851, Finland (ilya.petrov@lut.fi, paula.immonen@lut.fi, juha.pyrhonen@lut.fi).

demagnetization of the permanent magnets.

In this paper, a self-holding three-position electric tubular actuator (SHTPETA) is proposed to be applied in the shifting of two preset gears (having different gear ratios) and a neutral point. The tubular structure is selected as it has less permanent magnet (PM) flux leakage, a higher power density, and an absence of asymmetric pull force between the mover and the armature [19]. The use of PM technology in the armature helps to achieve a high force density (similar to that in the actuators where PMs are located in the mover), and it also helps to achieve the no-load self-holding force, which is, in principle, impossible in linear induction machines [20]. The process of shifting the gears requires one neutral position to allow time for further synchronization of the rotating shaft with the rotating gear.

The paper is organized as follows. Section II addresses the construction and self-holding principle of the proposed actuator. Section III describes the design sequence of the actuator starting from a simple analytical approach to obtain the general dimensions and finalizing them by the finite element method (FEM) with more detailed geometry adjustments to achieve the highest possible self-holding force. Section IV discusses the operating and control principles of the actuator in the load condition. Section V verifies the results with the prototype. Section VI concludes the results.

II. Submission of a New Manuscript for Review

The proposed short-stroke linear actuator comprises the PM, two stationary cores, and two coils on the armature side as shown in Fig. 1. The mover has only one active electromagnetic element, which is a solid core made of constructional steel allowing relatively high eddy currents in the core. However, these eddy currents are not very harmful in an occasional working cycle of the actuator. The first and second armature cores can also be made of the same constructional steel material as the mover core. It can be seen that the structure of the proposed actuator is similar to the flux-switching permanent magnet synchronous machines (FSPMSM), which have gained in popularity over the past few decades owing to their simple rotor structure [21], relatively high synchronous inductance [22], fault tolerance [23], an option to apply sensorless control [24], direct heat dissipation from the winding and magnets through the stator structure [25], and competitive torque/power density [26]. The proposed SHTPETA has some of these advantages related to the simple and robust mover structure, favorable thermal management, and competitive force density. The force/power density of the proposed linear actuator compared with more traditional linear machines should also be at a competitive level, because the tangential stress produced in the SHTPETA follows the same principle as in FSPMSMs, and therefore, the level of tangential stress should remain the same. For comparison, a two-position actuator (outlined in [9]) of a similar size to that of the SHTPETA produces about 230 N of peak force and only about 5 N of self-holding force, whereas the SHTPETA was measured to produce about 250 N of peak force and 100 N of self-holding force, even though the measured results of

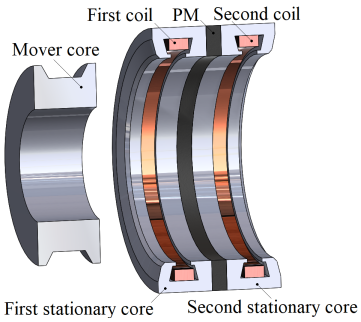

Fig. 1. Half-cut schematic view of the proposed SHTPETA.

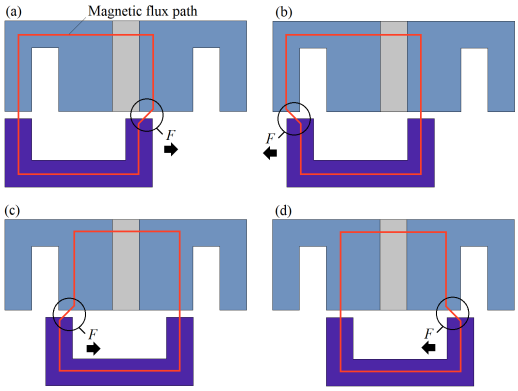

Fig. 2. Origin of the self-holding force F in the SHTPETA (a) when the mover is in the leftmost position and it is moved to the left, (b) when the mover is in the leftmost position and it is moved to the right, (c) when the mover in the middle and it is moved to the left, and (d) when the mover is in the middle position and it is moved to the right.

the SHTPETA are significantly degraded from the theoretical analysis for assembly reasons described below.

The idea behind the self-holding principle is similar to the occurrence of cogging force in traditional linear actuators. The origin of these forces is the magnetic saliency in the stator and (or) rotor structures produced by slot openings. This magnetic saliency generates a reluctance force, which tries to reach a position where the lowest value of magnetic reluctance is found. The principle of this phenomenon is illustrated in Fig. 2. It should be noted that the basic geometry shown in Fig. 2 only represents a schematic visualization of the actuator to describe the origin of the self-holding force in the SHTPETA, while the final geometry of the designed actuator can have quite different modifications as a result of differently shaped magnets, slots, and teeth on the armature and mover sides. However, the main force generation principle remains the same; the surfaces of different actuator components that face the air gap remain in the same order and occupy a similar proportion of the overall active electromagnetic surface. In Figs. 2 (a) and (b), a self-holding force is generated to hold the mover in the leftmost position, preventing it to move further to the left (a) or to the right (b). In Figs. 2 (c) and (d), a self-holding force is generated to keep the mover in the middle position, preventing it to move either to the left (c) or to the right (d).

This type of self-holding force in three different positions of

the mover can be achieved if three locations are found where the magnetic reluctance between the mover and the armature is at the minimum and it increases as a gradient of the mover distance from these positions. Such a condition is achieved if both the teeth of the mover oppose the maximum core area of the armature. In the case of the rightmost or leftmost position of the mover, as shown in Figs. 2 (a) and (b), the area of the mover core facing the armature core is reduced when the mover changes its position to the left or to the right. The same holds true when the mover is located in the middle of the armature, Figs. 2 (c) and (d). When the mover is moved in both directions (right or left) from the middle position, one of the mover teeth starts to face the armature slot opening, which increases the magnetic reluctance and consequently, generates force against the movement. These magnetic conditions allow to achieve self-holding forces in three mover positions.

III. Design sequence

Owing to the advanced commercial FEM tools that are able to build and analyze a model with acceptable precision (in the axisymmetric 2D domain), taking into account the fringing effect and any asymmetric displacements [19], the design of tubular actuators is usually based on the FEM, which is applied to determine the no-load characteristics along with the dynamic response to the load control signals. However, a very initial analytical design approach is preferred to estimate the primary dimensions of the main electromagnetic components of the actuator before the development of the FEM model is started. Therefore, the initial dimensions of the proposed SHTPETA are found by simple analytical equations based on the required stroke distance (with certain assumptions) and then, the design is followed by FEM simulations with more detailed adjustments to the actuator dimensions. The algorithm with the following design steps is shown in Fig. 3, where all the steps of the algorithm are assigned sections and subsections of their own in the paper.

In Fig. 3 it can be seen that the preliminary analytical design is based on the required distance to be moved, followed by a FEM analysis to take into account the fringing effect and possible flux leakage. Then, the no-load self-holding force is adjusted by optimizing the armature slot, magnet, and middle armature teeth widths. Afterward, all the widths of the active components are scaled to eliminate the error between the resultant stroke distance and the targeted one. Finally, the load condition is analyzed by selecting the required number of turns and applying the preset voltage value. The proposed design approach aims to achieve the final design solution of the SHTPETA within a relatively fast design procedure. It mainly comprises identification of several geometric parameters of the actuator (one-by-one) by their simple sweeping followed by initial analytical computation. Naturally, each design step shown in Fig. 3 or even the whole design sequence can be replaced by more advanced optimization procedures (e.g. an optimization approach applying a Pareto front). However, considering the large number of initial parameters, these optimization methods are assumed to require too heavy computational resources, and the effect of certain geometric parameters on

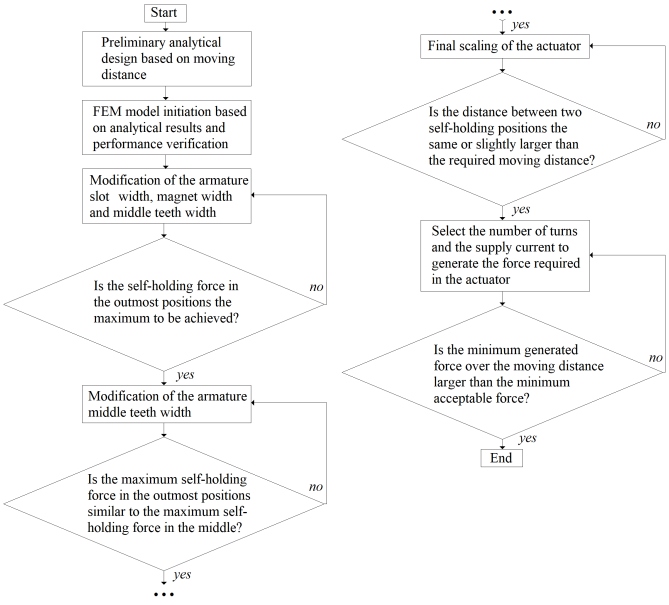

Fig. 3. Sequential algorithm of the SHTPETA design procedure.

particular actuator performance characteristics might not be that evident. In contrast, the results of the sweeping procedure clearly indicate how certain geometrical modifications of the actuator affect any given performance characteristics. The reason why the no-load condition is first analyzed (when only the self-holding force takes place) is the need to achieve a design solution that has three apparent self-holding positions.

A. Preliminary analytical design based on the moving distance

Based on [27], the highest reluctance force is achieved in a synchronous reluctance machine (SRM) when the angle between the peak current linkage and the rotor position with the lowest reluctance is 45 electrical degrees. Similar phenomena are observed in a linear actuator that contains an armature with two teeth and a mover with one tooth (providing the path for the magnetic flux) having an equal width of all elements (the armature teeth, the armature slot, and the mover tooth) as shown in Fig. 4. Three mover positions shown in Figs. 4 (a), (c), and (e) have a zero force, and two mover positions (located at equal distances from the zero force positions) have the highest force. The highest force is found when the position of the mover tooth is shifted by half of the slot width ($0.5x$), Figs. 4 (b) and (d).

Following the logic described above, an actuator having the main dimensions shown in Fig. 5 is taken as a starting point for the SHTPETA design. The main principle is that when one tooth of the mover completely faces the armature core area, then another tooth is shifted by half of the slot width. In that case, with the assumption of no fringing effect and no flux leakage (when the magnetic flux travels strictly in the vertical direction in the air gap), this provides the highest force with the minimum required space. Naturally, the fringing effect is very important for these types of machines, and therefore, in terms of the maximum achievable force, the evaluated results

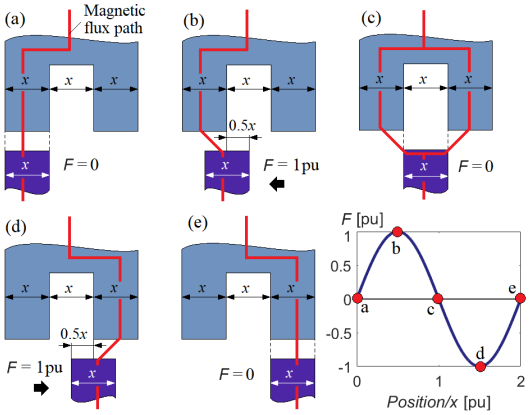

Fig. 4. Principle of force generation in a linear actuator having two teeth and a mover containing one tooth. x is the width of the armature teeth, slot, and mover tooth.

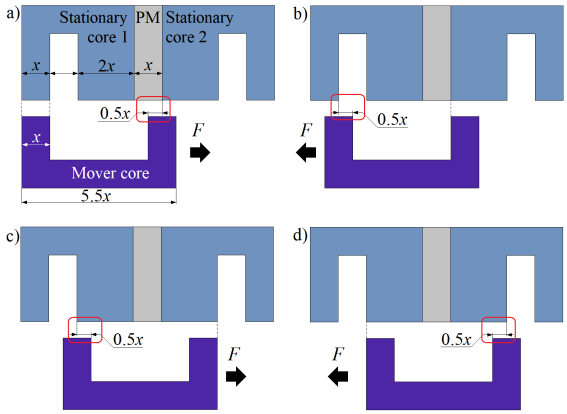

Fig. 5. Selection of the initial SHTPETA main dimensions and the direction of the self-holding force of the actuator in different mover positions. (a) The mover is slightly shifted to the left from the leftmost self-holding position, (b) the mover is slightly shifted to the right from the leftmost self-holding position, (c) the mover is slightly shifted to the left from the middle self-holding position, and (d) the mover is slightly shifted to the right from the middle self-holding position.

without the fringing effect cannot be treated as the final actual performance characteristics of the actuator (as will be shown below). However, this initial design approach can be used for relatively fast and simple evaluation of the approximate length of the actuator (armature length and mover length) to achieve the required stroke distance.

If the main initial dimensions of the actuator are selected as in Fig. 5, the zero force at no load is found in the mover positions shown in Fig. 6. It can be seen that in both mover positions (leftmost and middle) there is a certain shift ($0.25x$) of the mover teeth relative to the armature teeth. In this case, the relation of the stroke mover distance l_{stroke} to the armature slot width x (which is initially the same as the armature and mover teeth widths) can be found as

$$l_{\text{stroke}} = -0.25x + 2x - 0.25x = 1.5x, \tag{1}$$

$$x = \frac{2l_{\text{stroke}}}{3}, \tag{2}$$

For an ideal case assuming no fringing effect and zero flux leakage, it suffices to use (1) and (2) to select the

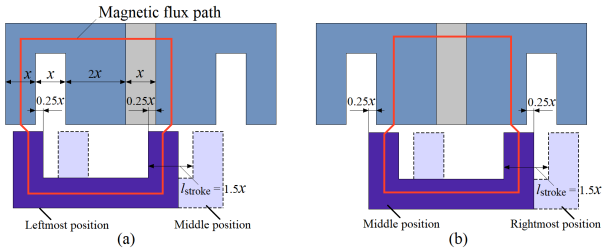

Fig. 6. (a) Leftmost self-holding mover position with the magnetic flux path and (b) middle self-holding mover position with the magnetic flux path; the no-load force is zero in this position.

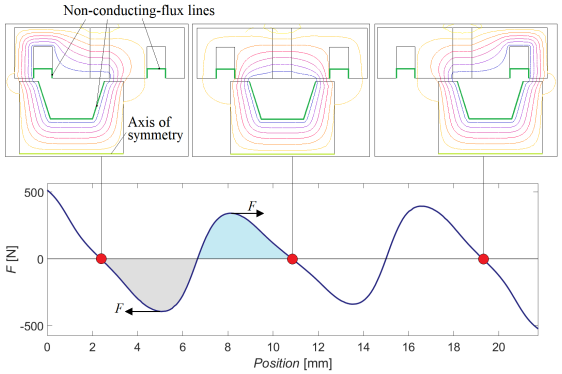

Fig. 7. Distribution of flux lines in the actuator in the leftmost, middle, and rightmost positions with the no-load force as a function of mover position. 2D axisymmetric FEM.

armature tooth width, armature slot width, and the mover tooth width (which are the same at this stage). This step is the initial analytical design based on the moving distance in the algorithm in Fig. 3. The required stroke distance for which the proposed SHTPETA is designed is $l_{\text{stroke}} = 8.6$ mm, and thus, the armature tooth width, the armature slot width, and the mover tooth width are estimated to be $x = 2l_{\text{stroke}}/3 = 2 \times 8.6/3 = 5.73$ mm.

B. FEM model initiation based on analytical results

To verify the self-holding force generated in the actuator in different mover positions (assuming no flux leakage and no fringing effect), a model was built and analyzed by the FEM (using the Altair Flux 2019 software package) with the following boundaries. The slot area in the armature and the slot area in the mover do not conduct magnetic flux by applying nonconducting flux lines indicated by green color in Fig. 7. The mover and armature cores are made of structural steel S355, which is often applied in solid rotor cores of high-speed induction machines [28]. The permanent magnet grade is 38SH, which should have about 1.15 T remanent flux density at 100° C and up to 1.22 T at 20° C. The distribution of magnetic flux lines and the no-load force as a function of mover position are shown in Fig. 7. The positive force is directed to the right and the negative force to the left.

It is noteworthy that the radial dimensions (i.e., the outer diameter of the actuator) are also optimization parameters that affect the overall characteristics of the actuator. For example, if the armature core is adjusted to have a larger outer diameter

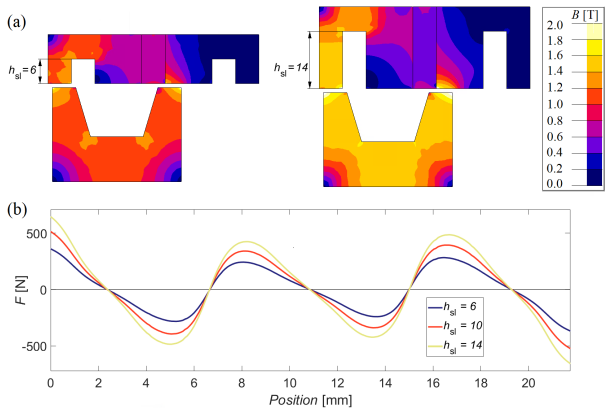

Fig. 8. a) Flux density distribution in the actuators with different radial dimensions obtained by adjusting the slot height h_{sl} (the color bar is valid for both models), and b) no-load self-holding force as a function of mover position for the actuators having three different slot heights. 2D axisymmetric FEM.

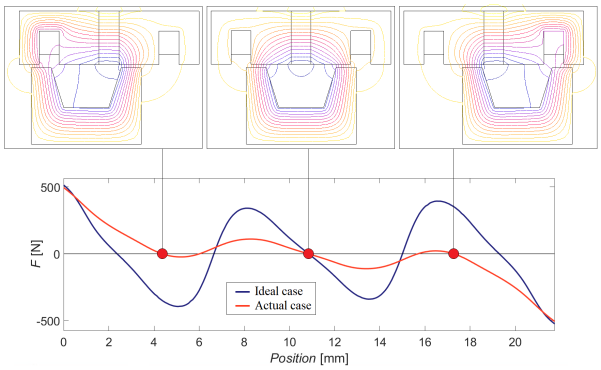

Fig. 9. Flux line distribution in the actuator in the leftmost, middle, and rightmost positions removing specific boundary conditions, and the no-load force as a function of the mover position of the model without the fringing effect (Ideal case) in comparison with the no-load force of the model after removing the specific boundaries (Actual case). 2D axisymmetric FEM.

by increasing the slot height, as it is shown in Fig. 8 (a), the values of flux density over the armature core and the mover core will increase, which is quite natural as the permanent magnet area increases. Further, the maximum values of the self-holding force and the force/position ratio (force gradient as a function of mover position) also increase, Fig. 8 (b). However, the positions where the self-holding force is zero (self-positioned points) remain in the same place, which means that the radial dimensions of the actuator do not affect the self-holding positions, but can be used to adjust the values of the self-holding force (along with values of the load force, as will be shown below). In the application for which the actuator under study is designed (a clutch system) there are no strict requirements for stiffness (force/position ratio). However, as it is shown in Fig. 8, this characteristic can be adjusted by modifying the radial dimensions. At this stage, the slot height is selected to be $h_{\mathrm{sl}} = 10$ mm, which meets the requirements of the outer radial dimensions, and does not cause any saturated regions in the armature core.

Figs. 7 and 8 show that the peak value of the self-holding forces in the leftmost and rightmost positions is not far away from the peak value of the self-holding forces in the middle position, indicating that the initial design approach based on (1) and (2) gives reasonable results in terms of self-holding force distribution over the mover positions. However, in reality, because of the fringing effect and the flux leakage, the no-load force can be significantly affected by removing the boundaries (nonconducting flux lines) set in the first model, as shown in Fig. 9. The no-load force in the actual case (after removing the boundaries set in the first model) is significantly reduced. Especially the self-holding force in the leftmost and rightmost positions is very small. The flux leakage and the fringing effect can be seen in the flux line distributions in Fig. 9, where some of the magnetic flux lines travel from the mover tooth in the leftmost position to the middle tooth of the armature core, which produces an adverse effect significantly reducing the value of the no-load self-holding force. The same situation occurs when the mover is in the rightmost position.

C. Modification of the armature slot width, magnet width, and middle teeth width

In order to reduce an adverse fringing effect, it is possible to decrease the mover tooth width by keeping the outer mover dimensions the same and follow the initial rule according to which only half of the mover tooth faces the armature core (tooth) while the whole another mover tooth faces the armature core (tooth) in all three positions (leftmost, middle, and rightmost). It should be noted that the reduction of the mover tooth width by $\Delta x_{\mathrm{t.mov}}$ is made from the mover inner slot area (to keep the outer dimensions of the mover the same). In this case when the mover is located in the leftmost position as shown in Fig. 10 (a), after the reduction of the mover tooth width by $\Delta x_{\mathrm{t.mov}}$, the overall armature length between these mover teeth (comprising the slot, middle tooth, and PM) should increase by $\Delta x_{\mathrm{t.mov}} + 0.5\Delta x_{\mathrm{t.mov}} = 1.5\Delta x_{\mathrm{t.mov}}$. However, when the mover is located in the middle position as shown in Fig. 10 (b), after the reduction of the mover tooth width by $\Delta x_{\mathrm{t.mov}}$, the overall armature length between these mover teeth (comprising two middle teeth and PM) should increase only by $0.5\Delta x_{\mathrm{t.mov}}$. In addition, it should be borne in mind that the PM width and armature slot width should be increased and the middle armature tooth should be decreased in the modification to maintain the reduction in the fringing effect. Therefore, considering the above, the following equations can be composed to estimate changes in the armature middle teeth width $\Delta x_{\mathrm{t.mid.arm}}$, the PM width Δx_{PM}, and the armature slot width $\Delta x_{\mathrm{sl.arm}}$ as a function of reduction in the mover tooth width (keeping the PM width and the armature slot width equal to each other):

$$1.5\Delta x_{\mathrm{t.mov}} = \Delta x_{\mathrm{sl.arm}} + \Delta x_{\mathrm{PM}} + \Delta x_{\mathrm{t.mid.arm}}, \quad (3)$$

$$0.5\Delta x_{\mathrm{t.mov}} = \Delta x_{\mathrm{PM}} + 2\Delta x_{\mathrm{t.mid.arm}}, \quad (4)$$

$$\Delta x_{\mathrm{t.mid.arm}} = -\frac{\Delta x_{\mathrm{t.mov}}}{6}, \quad (5)$$

$$\Delta x_{\mathrm{sl.arm}} = \Delta x_{\mathrm{PM}} = \frac{5\Delta x_{\mathrm{t.mov}}}{6}, \quad (6)$$

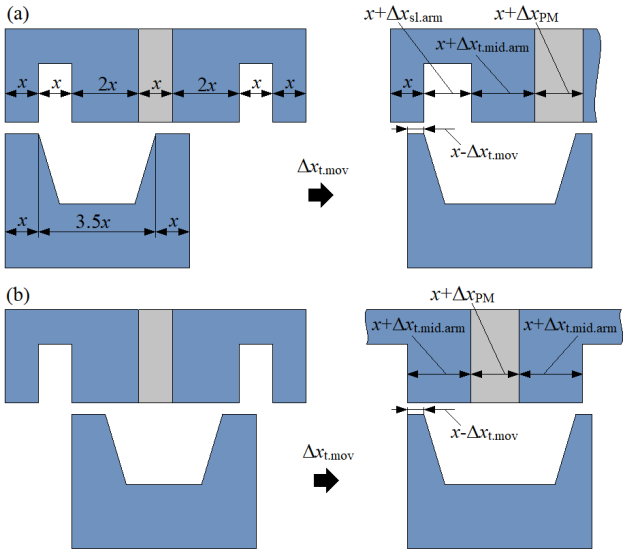

Fig. 10. Modification of the actuator geometry to reduce the fringing effect by decreasing the mover tooth width. (a) Overall increase in the armature length when the mover is located in the leftmost position and (b) overall increase in the armature length when the mover is located in the middle position.

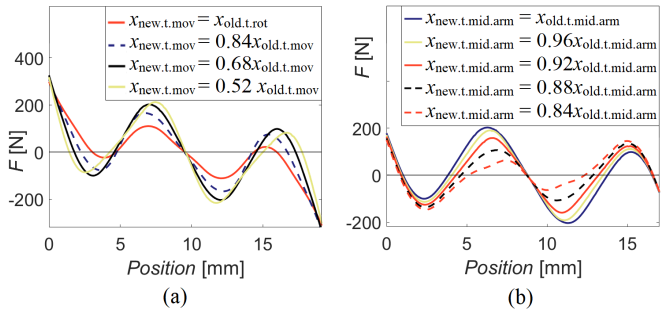

Fig. 11. (a) No-load forces at different mover tooth widths, and (b) no-load forces at different middle armature teeth widths (when increasing the armature slot width to the same extent as the middle armature tooth width is reduced). 2D axisymmetric FEM.

First, (3) and (4) containing two unknowns ($\Delta x_{\mathrm{sl.arm}} = \Delta x_{\mathrm{PM}}$ and $\Delta x_{\mathrm{t.mid.arm}}$) are solved, after which the relation of the armature slot width (together with the PM width) and the relation of the armature middle tooth width to the reduction in the mover tooth width is found by (5) and (6). This relation is taken into account when the mover tooth width is reduced. Fig. 11 (a) shows the change in the no-load self-holding force as a function of mover position at different mover tooth widths, upgrading all the other dimensions by (5) and (6). Based on the figure, the best option for the mover tooth width reduction is at 68% of the initial tooth width, which gives a peak self-holding force of 101 N in the leftmost position and a peak self-holding force of 203 N in the middle position, being 420% and 183% of the initial peak self-holding forces of the actuator, respectively.

D. Modification of the armature middle teeth width

After the mover tooth adjustment, the peak self-holding force in the middle (203 N) is about twice as high as the self-holding force in the leftmost and rightmost positions (101 N). In order to make their values closer to each other, it is possible to reduce the width of the armature middle teeth while increasing the armature slot width to the same extent. In this case, the fringing effect through the armature slot is reduced, which should increase the peak self-holding force in the leftmost and rightmost positions. However, at the same time, the peak self-holding force in the middle position should decrease as a result of not following the initial rule according to which one mover tooth fully faces the armature core, and at the same time, the other mover tooth faces half of the armature core. In the case of the middle armature teeth reduction, one mover tooth (when the mover is in the middle) faces less than half of the armature core keeping the other mover tooth fully covered by the armature core. This is verified by the FEM analysis shown in Fig. 11 (b). The figure shows that the peak self-holding force of the leftmost or rightmost positions increases with a reduction in the middle armature tooth width. However, at the same time, the peak self-holding force in the middle decreases relatively fast with a smaller middle armature tooth width. The new armature middle tooth width $x_{\mathrm{new.t.mid.arm}}$ was selected to be 92% of the initial armature middle tooth width $x_{\mathrm{old.t.mid.arm}}$ as it still gives a considerable gain in the peak self-holding force in the leftmost and rightmost positions (125 N) while not loosing too much of the peak self-holding force in the middle (158 N).

E. Final scaling of the actuator

After all the geometry adjustments have been made to achieve the highest self-holding force, it has to be checked if the new resultant stroke distance from the leftmost self-holding position to the middle self-holding position and to the rightmost self-holding position is the same as it was initially selected. In the studied case, the resultant stroke between the leftmost position to the middle is 7.78 mm, while initially, the required stroke distance was 8.6 mm. In order to adjust the actual stroke distance to the required value, a simple scaling can be applied. In the SHTPETA, the stroke distance increases linearly with the scaling of the widths of all the actuator elements. This means that the width of all the components (armature teeth, armature slot, PM, mover tooth, mover slot) should be increased by $(8.6/7.78) \times 100\% - 100\% = 10.5\%$ to reach the required stroke distance. The final actuator dimensions and no-load characteristics before and after scaling are listed in Table I. According to the results listed in Table I, not only the overall stroke distance has changed but also the peak self-holding force has increased after the scaling up of the widths of the components. For the studied application, an increased self-holding force after the scaling is preferred. However, if the force characteristics of the actuator have to be the same after the scaling, this can be achieved by reducing the radial dimensions of the armature until the force reaches the required level in the same way as shown in Fig. 8.

After the scaling, when the stroke distance requirements are met, it is possible to modify the armature geometry to simplify the manufacturing process and increase the armature slot area as shown in Fig. 12. The figure shows that if all

TABLE I
DIMENSIONS AND NO-LOAD CHARACTERISTICS OF THE ACTUATOR BEFORE AND AFTER SCALING

Parameter	Before scaling	After scaling
Mover length	31.5 mm	35 mm
Air gap (defined by requirement)	1 mm	1mm
Armature length	55.5 mm	61.6 mm
Peak outermost position force	125 N	160 N
Peak middle position force	158 N	184 N
Stroke distance (outermost to middle)	7.78 mm	8.6 mm
Mover outer diameter	106 mm	106 mm
Armature inner diameter	108 mm	108 mm
Armature outer diameter	140 mm	140 mm
Armature slot height	10 mm	10 mm
Mover slot height	12 mm	12 mm

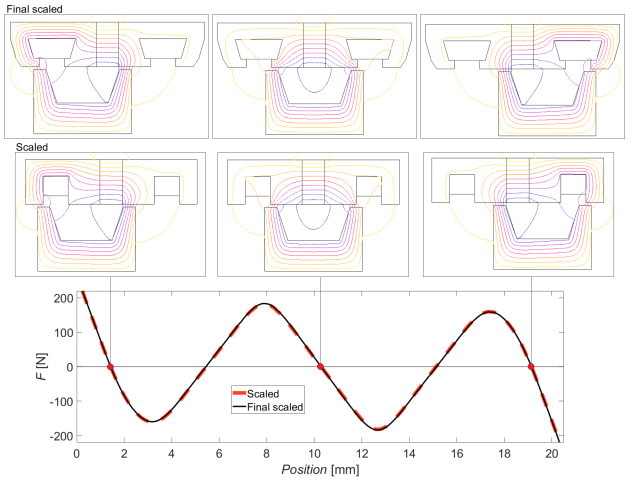

Fig. 12. Final actuator geometry with adjusted slot area and armature teeth shape in comparison with the initial scaled actuator with no-load forces as a function of mover position. 2D axisymmetric FEM.

the widths of the actuator components that face the air gap are kept unchanged by careful modification of the rest of the armature geometry (avoiding saturation in the magnetic circuit), it is possible to achieve exactly the same no-load self-holding force as a function of mover position. At the same time, the modification of the armature geometry can be based on keeping the current density in the slot winding at a reasonable value. For example, if the supply current is too high in the original slot area and the radial dimension of the actuator cannot be modified, then the modification of the final geometry depicted in Fig. 12 can be adjusted accordingly. This final update can be considered a device-oriented modification, which is carried out outside the main design sequence (shown in Fig. 3) to fit the application needs. As a conclusion to this design step, it can be added that the optimum geometrical dimensions may, in principle, vary with different requirements, but the described algorithm sequence allows to find a design with the highest self-holding forces.

IV. OPERATING PRINCIPLES AND LOAD CHARACTERISTICS

The next step is to select the number of turns, supply current, and current density applied to the actuator in the load

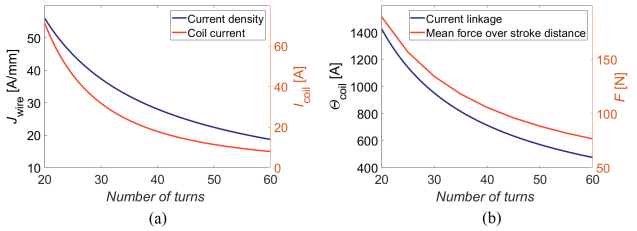

Fig. 13. (a) Supply current and current density as a function of the number of turns, (b) mean force over the whole stroke distance and current linkage as a function of the number of turns. 2D axisymmetric FEM.

condition. It was found that the minimum current linkage of 720 A should be induced by each coil to exceed the self-holding force in any mover position. Therefore, this current linkage is assumed the minimum value required to generate the force in the needed direction in any mover position.

The DC voltage supply required by the application is 25 V. Knowing the total area of the coil (64.1 mm^2) and the copper space factor (0.4), it is possible to evaluate the resistance of the coil, supply current, current density, current linkage, and the total power loss in the coil as a function of the number of turns. The resistance of the coil is the main limitation on the maximum supply current and thereby, on the current density. With a higher number of turns, the resistance increases and the supply current, current linkage, and current density decrease. Fig. 13 (a) shows the supply current and the current density as a function of the number of turns. The mean force over the whole stroke distance and the current linkage in the coil as a function of the number of turns are shown in Fig. 13 (b). Considering the required current linkage (at least 720 A), it is found that the number of turns per coil should be at least 40 to reach this current linkage. With this number of turns, the supply current is 18 A, the current density is 28 A/mm^2, the coil resistance is 0.7 Ohm, the mean force over the whole stroke distance is 108 N, and the electrical power consumed by one coil is 225 W. This current density is fully acceptable if it can be assumed that the working duty cycle of this actuator is not higher than the duty cycle of a typical passenger car over a standard driving cycle, which is 3% [8]. The assumption of the acceptable current density was partially verified during the measurement sequence, where the temperature of the frame did not exceed 100° C during the interrupted working condition. However, a detailed thermal analysis of the SHTPETA is outside the scope of this paper.

In order to generate the force in a particular direction in the SHTPETA, a DC voltage source has to be applied to each coil with a certain polarity. An example of the application of polarity to each coil to generate the required direction of force is shown in Fig. 14. The flux lines in different mover positions when the force is generated to the right and to the middle are shown in Figs. 15 (a) and (b), respectively. The values of the forces (no-load force and forces in different directions) as a function of mover position are shown in Fig. 15 (c). It can be seen in the figure that it is possible to generate only positive or negative force over the whole stroke length (from the leftmost to rightmost mover positions). However, the value

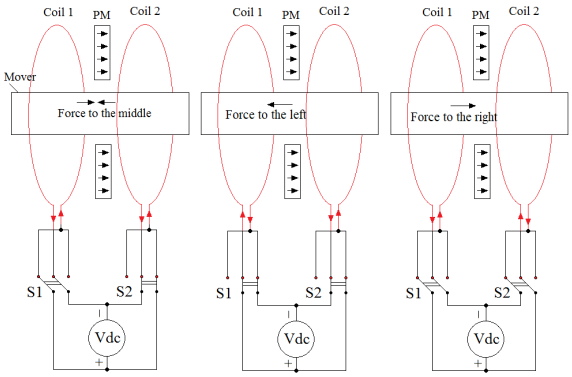

Fig. 14. Control of the SHTPETA to generate the force in different directions.

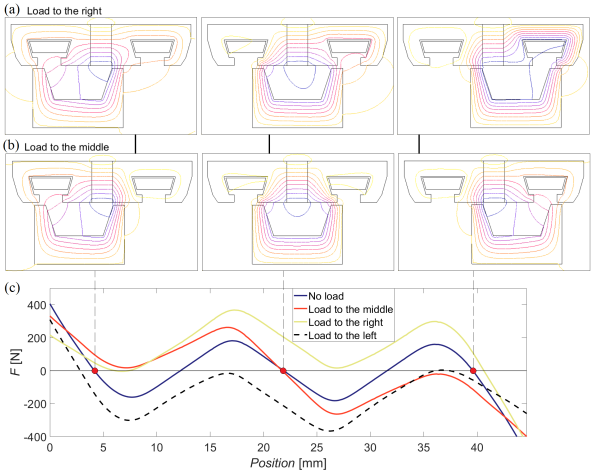

Fig. 15. Magnetic lines in three fixed mover positions when (a) the force in the mover is directed to the right, and (b) the force in the mover is directed to the middle. (c) No-load and load forces as a function of mover position. 2D axisymmetric FEM.

of the forces is not constant over the mover distance because of the strong effect of the self-holding force. According to the FEM results shown in Fig. 15 (c), to exceed the self-holding force in the designed actuator, at least 18 A of DC current has to be applied. However, if the self-holding force is too strong in certain designs, it is still possible to reduce it by applying different widths of the mover teeth, armature slot width, and armature middle tooth width. For this particular design, the load force is enough to make the required gear couplings, and therefore, the actuator was not further modified.

The overall reliability of the proposed actuator is also demonstrated in Fig. 15, which shows that the configuration significantly reduces the risk of irreversible demagnetization of the magnets by the parallel magnetization of the magnet relative to the armature reaction. Therefore, the flux lines in the magnet shown in Fig. 15 are not distorted by the armature flux. In addition, the temperature of the magnet can be regulated more easily when the magnet is positioned directly in the stator. Further, when the mover contains only the steel element (without permanent magnets), it becomes much less vulnerable to highly dynamic working conditions.

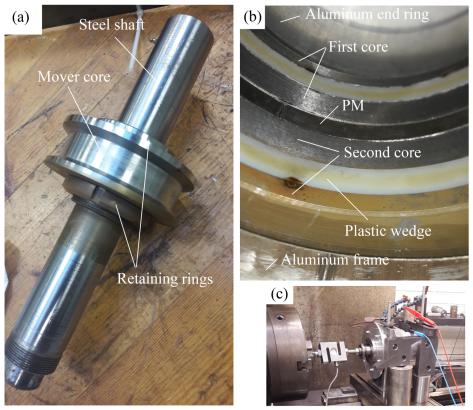

Fig. 16. (a) Mover, (b) stationary unit, and (c) test bench of the SHTPETA.

V. Verification of the Proposed Linear Actuator by Measurements

The designed actuator was constructed based on the dimensions obtained from the final design step with an increased slot area as shown in Fig. 12. The mover and the stationary unit are shown in Figs. 16 (a) and (b). The stator core containing two teeth could not be made as a single unit. Therefore, the stator yoke and both the teeth were made as separate elements glued to each other. The stator cores were glued to the PM and assembled to the aluminum housing. The test setup is shown in Fig. 16 (c), which contains the force sensor (Raute TB5-1000kg-C1), the DC voltage (current) supply, and the precise mover positioning system rearranged from the chuck of the milling machine.

The initial measurements revealed that the measured results do not match the results obtained by the 2D axisymmetric FEM simulations. Therefore, the FEM model had to be modified to match the measured results. However, the modified parameters partially agree with the actual manufacturing conditions (e.g. glued stator core elements and the smaller actual remanence of the PM). The final FEM model is shown in Fig. 17. It can be seen in the figure that extra air gaps (0.2 mm) were added to the model between all the glued elements of the stator. Further, the magnet remanence was reduced to 0.8 T, while the air gap length was reduced to 0.9 mm.

The final version of the SHTPETA has quite a different overall geometry from the initial schematic view of the actuator depicted in Fig. 2, where in the updated version of the actuator the shapes of the slots and the teeth are different. This is a result of a detailed analysis of the utilization of the magnetic core within the actuator, where the areas of the cores with less effective use (e.g. where the flux density remains relatively low) are replaced with either air or an extra copper area. Further, an extra armature slot area is achieved by modifying the upper region of the edge teeth. However, these modifications do not change the region where the main electromagnetic interaction occurs (the air gap), and thus, the same stroke distance and force values as shown in Fig. 12 are maintained. This means that (1)–(6), which are used to determine the initial design of the SHTPETA, are still valid for the final geometry modification, as their main applicability

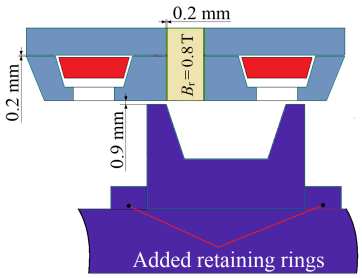

Fig. 17. Final 2D axisymmetric FEM model, the simulated results of which were compared with the measured results.

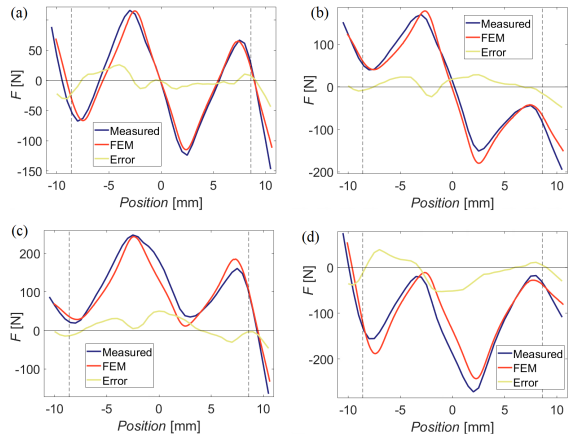

Fig. 18. (a) No-load force, (b) load force toward middle, (c) load force toward left, and (d) load force toward right. The 2D axisymmetric FEM-simulated results are compared with the measured results.

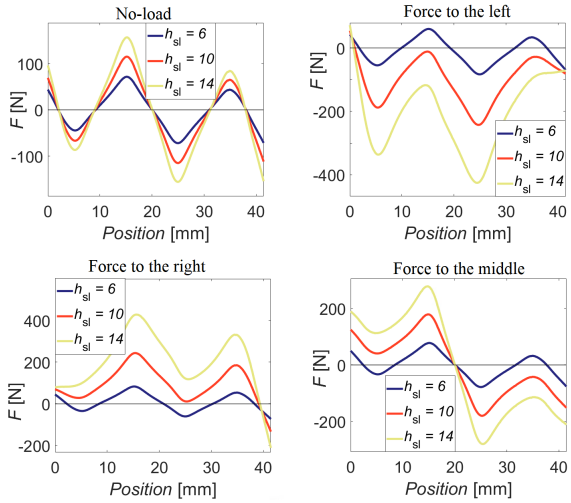

Fig. 19. No-load self-holding force as a function of mover position for the actuators with three different slot heights. The supply currents applied to the FEM models were 2 A, 18 A, and 34 A for the 6 mm, 10 mm, and 14 mm slot heights, respectively. 2D axisymmetric FEM.

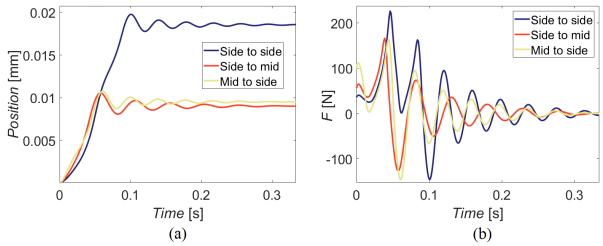

Fig. 20. (a) Position and (b) force as a function of time during the switching from one position to another. The total mass of the mover is 4.5 kg, which corresponds to the actual measured mass of the mover. 2D axisymmetric FEM.

is still related to the areas that face the air gap (where the main electromagnetic interaction occurs).

The results obtained from the simulation of the 2D axisymmetric FEM model are compared with the measured results in Fig. 18. A good agreement between the simulations and the measurements can be observed in all four load conditions, where a significant proportion of the mismatch between the simulated and measured results occurs as a result of the phase shift error rather than the force amplitude error. In total, there are three apparent self-holding positions, while the no-load self-holding force is above 50 N, as was defined by the requirements. The direction of the required load force remains unchanged along the whole possible mover distance, which ensures the correct final destination of the mover depending on the current polarity applied to the coils.

The resultant stroke distance shown in Fig. 18 between the two self-holding positions at no-load is about 5% longer than required by the application distance. However, this is acceptable, because there are special supporting units in the actual device, which prevent the mover from exceeding the required outermost positions. Further, when the load force is applied toward the outermost mover positions, it remains quite strong even when the required positions are reached. This is similar to the initially simulated results shown in Fig. 15, and it is considered an applicable feature of the actuator to make sure that the mover reaches the desired outermost positions even if some external load opposes the motion.

As it can be seen in Fig. 18, the measured performance of the actuator satisfied the requirements set by the application. However, there is one relatively simple method to improve the characteristics of the actuator if the original design does not meet the requirements. This method was presented at the beginning of the paper, and it is related to adjustment of the stator slot height. Fig. 19 demonstrates how the characteristics of the final design solution of the actuator would change when applying different slot heights in the design, where along with the height of the armature slot also the supply current is adjusted to keep the same current density in the slot winding. The original slot height of the designed actuator was $h_{\mathrm{sl}} = 10$ mm. Fig. 19 shows that using a shorter slot can lead to a case where the required characteristics are not achieved. At the same time, using a larger slot height helps to increase the maximum achievable force both in no-load and load conditions because of the larger permanent magnet surface area and the opportunity to supply higher current to a larger slot area.

The simulated results of the final FEM model with coupled load kinematics (Flux 2019) are shown in Fig. 20, with the focus on the dynamic response of the mover when using the simple control principle (in which the DC voltage is directly applied to the terminals of the actuator). The figure shows the

mover position and the force applied to the mover during the switching condition. These results of the switching sequence were validated by measurements (without any external load attached), where it took about 0.05 s to switch from the middle position toward the outermost positions, and the same time to switch back. Further, it took about 0.1 s to switch from one outermost self-holding position to another.

VI. Conclusion

A self-holding three-position actuator that was initially designed for a two-step transmission in an electric vehicle meets the requirements of applying a self-holding force above 50 N for the maximum stroke distance of 8.6 mm. The initial analytical design step described in the paper can be used for a rough estimation of the overall width of the actuator including the armature and mover widths. However, for more precise design adjustment, the FEM or more advanced analytical tools must be used. The proposed SHTPETA showed the capability to work with a simple control (applying only DC voltages), robust structure, and high self-holding forces.

References

[1] J. Goss, M. Popescu, and D. Staton, "A comparison of an interior permanent magnet and copper rotor induction motor in a hybrid electric vehicle application," in *2013 International Electric Machines Drives Conference*, DOI 10.1109/IEMDC.2013.6556256, pp. 220–225, May. 2013.

[2] S. De Pinto, P. Camocardi, A. Sorniotti, P. Gruber, P. Perlo, and F. Viotto, "Torque-fill control and energy management for a four-wheel-drive electric vehicle layout with two-speed transmissions," *IEEE Transactions on Industry Applications*, vol. 53, DOI 10.1109/TIA.2016.2616322, no. 1, pp. 447–458, Jan. 2017.

[3] W. Mo, P. D. Walker, Y. Fang, J. Wu, J. Ruan, and N. Zhang, "A novel shift control concept for multi-speed electric vehicles," *Mechanical Systems and Signal Processing*, vol. 112, DOI https://doi.org/10.1016/j.ymssp.2018.04.017, pp. 171 – 193, 2018.

[4] High Torque Capacity RWD Multi Stage Hybrid Transmission, 2019. [Online]. Available: https://www.aisin-aw.co.jp/en/products/drivetrain/lineup/hv.html

[5] J. Montonen, J. Nerg, M. Polikarpova, and J. Pyrhonen, "Integration principles and thermal analysis of an oil-cooled and -lubricated permanent magnet motor planetary gearbox drive system," *IEEE Access*, vol. 7, DOI 10.1109/ACCESS.2019.2919506, pp. 69 108–69 118, 2019.

[6] F. Baronti, A. Lazzeri, R. Roncella, R. Saletti, and S. Saponara, "Design and characterization of a robotized gearbox system based on voice coil actuators for a formula sae race car," *IEEE/ASME Transactions on Mechatronics*, vol. 18, DOI 10.1109/TMECH.2011.2162632, no. 1, pp. 53–61, Feb. 2013.

[7] M. Lindner and T. Tille, "Design of highly integrated mechatronic gear selector levers for automotive shift-by-wire systems," *IEEE/ASME Transactions on Mechatronics*, vol. 15, DOI 10.1109/TMECH.2009.2036171, no. 6, pp. 961–968, Dec. 2010.

[8] A. Turner, K. Ramsay, R. Clark, and D. Howe, "Direct-drive electromechanical linear actuator for shift-by-wire control of an automated transmission," in *2006 IEEE Vehicle Power and Propulsion Conference*, DOI 10.1109/VPPC.2006.364317, pp. 1–6, Sep. 2006.

[9] P. Immonen, V. Ruuskanen, and J. Pyrhonen, "Moving magnet linear actuator with self-holding functionality," *IET Electrical Systems in Transportation*, vol. 8, DOI 10.1049/iet-est.2017.0079, no. 3, pp. 182–187, 2018.

[10] A. J. Taberner, N. B. Ball, N. C. Hogan, and I. W. Hunter, "A portable needle-free jet injector based on a custom high power-density voice-coil actuator," in *2006 International Conference of the IEEE Engineering in Medicine and Biology Society*, DOI 10.1109/IEMBS.2006.260243, pp. 5001–5004, Aug. 2006.

[11] L. Encica, J. Makarovic, E. A. Lomonova, and A. J. A. Vandenput, "Space mapping optimization of a cylindrical voice coil actuator," *IEEE Transactions on Industry Applications*, vol. 42, DOI 10.1109/TIA.2006.882672, no. 6, pp. 1437–1444, Nov. 2006.

[12] L. Nascutiu, "Voice coil actuator for hydraulic servo valves with high transient performances," in *2006 IEEE International Conference on Automation, Quality and Testing, Robotics*, vol. 1, DOI 10.1109/AQTR.2006.254522, pp. 185–190, May. 2006.

[13] C. Noergaard, M. M. Bech, J. H. Christensen, and T. O. Andersen, "Modeling and validation of moving coil actuated valve for digital displacement machines," *IEEE Transactions on Industrial Electronics*, vol. 65, DOI 10.1109/TIE.2018.2808936, no. 11, pp. 8749–8757, Nov. 2018.

[14] T. J. Teo, H. Zhu, S. Chen, G. Yang, and C. K. Pang, "Principle and modeling of a novel moving coil linear-rotary electromagnetic actuator," *IEEE Transactions on Industrial Electronics*, vol. 63, DOI 10.1109/TIE.2016.2585540, no. 11, pp. 6930–6940, Nov. 2016.

[15] J. Wang, D. Howe, and Z. Lin, "Design optimization of short-stroke single-phase tubular permanent-magnet motor for refrigeration applications," *IEEE Transactions on Industrial Electronics*, vol. 57, DOI 10.1109/TIE.2009.2025710, no. 1, pp. 327–334, Jan. 2010.

[16] C. Pompermaier, K. Kalluf, A. Zambonetti, M. V. Ferreira da Luz, and I. Boldea, "Small linear pm oscillatory motor: Magnetic circuit modeling corrected by axisymmetric 2-d fem and experimental characterization," *IEEE Transactions on Industrial Electronics*, vol. 59, DOI 10.1109/TIE.2011.2161650, no. 3, pp. 1389–1396, Mar. 2012.

[17] F. Poltschak and J. Kobleder, "Design and optimization of a lightweight single phase linear actuator," in *The 10th International Symposium on Linear Drives for Industry Applications, At Aachen*, pp. 1–4, Sep. 2015.

[18] F. Poltschak and P. Ebetshuber, "Design of integrated magnetic springs for linear oscillatory actuators," *IEEE Transactions on Industry Applications*, vol. 54, no. 3, pp. 2185–2192, 2018.

[19] S. Miric, P. Kuttel, A. Tuysuz, and J. W. Kolar, "Design and experimental analysis of a new magnetically levitated tubular linear actuator," *IEEE Transactions on Industrial Electronics*, vol. 66, DOI 10.1109/TIE.2018.2868286, no. 6, pp. 4816–4825, Jun. 2019.

[20] M. Flankl, L. de Oliveira Baumann, A. Tuysuz, and J. W. Kolar, "Energy harvesting with single-sided linear induction machines featuring secondary conductive coating," *IEEE Transactions on Industrial Electronics*, vol. 66, DOI 10.1109/TIE.2018.2821637, no. 6, pp. 4880–4890, Jun. 2019.

[21] G. Zhang, W. Hua, and P. Han, "Quantitative evaluation of the topologies and electromagnetic performances of dual-three-phase flux-switching machines," *IEEE Transactions on Industrial Electronics*, vol. 65, DOI 10.1109/TIE.2018.2808908, no. 11, pp. 9157–9167, Nov. 2018.

[22] W. Hua, H. Zhang, M. Cheng, J. Meng, and C. Hou, "An outer-rotor flux-switching permanent-magnet-machine with wedge-shaped magnets for in-wheel light traction," *IEEE Transactions on Industrial Electronics*, vol. 64, DOI 10.1109/TIE.2016.2610940, no. 1, pp. 69–80, Jan. 2017.

[23] T. Raminosoa, C. Gerada, and M. Galea, "Design considerations for a fault-tolerant flux-switching permanent-magnet machine," *IEEE Transactions on Industrial Electronics*, vol. 58, DOI 10.1109/TIE.2010.2070782, no. 7, pp. 2818–2825, Jul. 2011.

[24] T. C. Lin, Z. Q. Zhu, K. Liu, and J. M. Liu, "Improved sensorless control of switched-flux permanent-magnet synchronous machines based on different winding configurations," *IEEE Transactions on Industrial Electronics*, vol. 63, DOI 10.1109/TIE.2015.2464303, no. 1, pp. 123–132, Jan. 2016.

[25] X. Cai, M. Cheng, S. Zhu, and J. Zhang, "Thermal modeling of flux-switching permanent-magnet machines considering anisotropic conductivity and thermal contact resistance," *IEEE Transactions on Industrial Electronics*, vol. 63, DOI 10.1109/TIE.2016.2522942, no. 6, pp. 3355–3365, Jun. 2016.

[26] P. Su, W. Hua, Z. Wu, Z. Chen, G. Zhang, and M. Cheng, "Comprehensive comparison of rotor permanent magnet and stator permanent magnet flux-switching machines," *IEEE Transactions on Industrial Electronics*, vol. 66, DOI 10.1109/TIE.2018.2875636, no. 8, pp. 5862–5871, Aug. 2019.

[27] J. Pyrhönen, T. Jokinen, and V. Hrabovcová, *Design of Rotating Electrical Machines*. New York: John Wiley Sons, 2008.

[28] C. Di, I. Petrov, and J. J. Pyrhonen, "Extraction of rotor eddy-current harmonic losses in high-speed solid-rotor induction machines by an improved virtual permanent magnet harmonic machine model," *IEEE Access*, vol. 7, pp. 27 746–27 755, 2019.

Ilya Petrov received the D.Sc. degree from the Lappeenranta University of Technology (LUT), Finland, in 2015. He is currently a Research Fellow of the Department of Electrical Engineering, LUT.

Paula Immonen received the M.Sc. degree in electrical engineering and the D.Sc. (technology) degree from the Lappeenranta University of Technology (LUT), Lappeenranta, in 2008 and 2013, respectively, where she is currently a Postdoctoral Researcher with the Department of Electrical Engineering. Her current research interest includes the diesel-electric hybrid drive systems in mobile working machines.

Juha Pyrhönen (M'06, SMâ17) was born in Kuusankoski, Finland, in 1957. He received the D.Sc. degree from the Lappeenranta University of Technology (LUT), Finland, in 1991. He became a Professor of electrical machines and drives with the LUT, in 1997. He is engaged in the research and development of electric motors and power-electronic-controlled drives. He has a wide experience in the research and development of special electric drives for distributed power production, traction, and high-speed applications. Permanent magnet materials and applying them in machines have an important role in his research. He is currently researching new carbon-based materials for electrical machines.